Extended Migdal-Watson formula to evaluate background strength in binary breakup reactions

R. Nakamoto [1], M. Ito [1], A. Saito [2] and S. Shimoura [3]

[1]*Department of Pure and Applied Physics, Kansai University, Yamatecho, 3-3-35, Suita 564-8680, Japan*
[2]*Department of Radiation Oncology, Hiroshima University Hospital, 1-2-3 Kasumi, Minami, Hiroshima, Hiroshima 734-8551, Japan*
[3]*Center for Nuclear Study, School of Science, University of Tokyo, 7-3-1, Hongo, Bunkyo-ku, Tokyo 113-0033, Japan*

A new formula to evaluate the nonresonant background for binary breakup is proposed by extending the Migdal-Watson (MW) formula, which was originally developed for s-wave breakup in charge neutral systems. The strength of the direct breakup, which is assumed by a one step transition from the initial bound state, is simulated by the complex scaling method (CSM) in binary cluster systems. The extended MW formula is applied to the direct breakup of ^{20}Ne $\rightarrow \alpha + ^{16}$O, and we have found that the formula nicely reproduces the strength of the direct breakup evaluated by CSM. We have demonstrated that new parameters introduced in the extended MW formula have a close connection to the spatial size of the initial wave packet, which is given by the product of the initial wave function and the external field. The application of the new formula to the direct breakup of ^{12}Be into $\alpha + ^{8}$He is also discussed.

I. INTRODUCTION

One of characteristic features in nuclear systems is a wide variety of nuclear structures in excited states. The properties of the ground state in the nuclei can be described by the mean-field structures [1] except for a few examples, hence the collective motion generated by the coherent single-particle excitation inside of the mean field appears in the excited states [1]. Furthermore, the so-called cluster structure induced by the decomposition of the nucleus into several subunits also exists in the excited states of the nucleus. The typical example of such a subunit is the α particle, and the nuclear structure based on the α particle is called the α cluster structure [2]. The α cluster model is well known to explain various features in lighter nuclei [2].

In the lighter mass systems, the difference in the mean-field and cluster structures is known to be prominent in excited states with lower spins, such as $J^\pi = 0^+$ and 1^-. In the mass region of $A \leqslant 20$, for instance, the 0^+ and 1^- states having cluster structures are observed as discrete or sharp resonant states in the lower excited states below the excitation energy of $E_x \leqslant 15$ MeV [3,4], while such lower spin states based on the mean-field structure exist in a much higher energy region, $E_x \geqslant 20$ MeV, with a broad width [1]. The experimental identification of the spin-parity and the decay width of the resonant states is essential to investigate the intrinsic structure of the observed resonances, which would be characterized in terms of the mean-field structure or the cluster structure.

Inelastic scattering is a useful tool to explore the nuclear structure in excited states. In particular, the inelastic excitation of the nucleus to the resonant states embedded in continua above the particle decay threshold, which is often called the breakup reaction, is very important because we can pin down the intrinsic nuclear structure in the resonances by controlling the detection of the exit channels, which are the combination of the emitted fragments [5–12]. For example, the nucleon decay must be the dominant process in the resonant states having a large probability of single-particle configurations [5–7], while the cluster decays, such as the α decays, will strongly occur in the resonances having a large component of the α cluster configuration [8–12]. Therefore, we can infer the features of the intrinsic structure in the resonant states through the observation of the breakup into the different channels, such as the cluster channels and the nucleon channels. A typical example of such a measurement of the different channels can be found in Ref. [13].

In recent studies, the breakup reactions going to the continuum states have been extensively advanced in both the experimental and theoretical fields. For example, the experimental technique to detect multiparticles decays including the decays of neutrons has been prominently developed [14–16], and this development allows deep investigation of the resonant states in the few-body continuum systems. In contrast, the famous example of the theoretical framework to handle the breakup reaction is known as the coupled discretized-continuum channel (CDCC) [17]. In recent studies, the CDCC method is more advanced. Sophisticated analyses have been done for binary [18] and three-body [19] breakup reactions. Moreover, it has been applied to complicated systems, including the mutual breakup process involving the multicluster configurations [20,21].

Good examples of the sophisticated analyses of the breakup reactions linked with the structure problem can be seen in the ^{12}Be nucleus, which finally decays into the $\alpha + ^{8}$He and ^{6}He $+ ^{6}$He channels [8–12]. In Ref. [10], a careful multipole decomposition analysis (MDA) was performed, and

the MDA analysis elucidates that many resonant states with an intermediate width of $\Gamma_R \leqslant 1$ MeV exist in the spins from $J^{\pi} = 0^+$ to 4^+ [10]. The resonances in these channels appear in a close energy spacing with $\Delta E \approx 0.5$ MeV in the lower excitation-energy region below $E_x = 15$ MeV. The experimental results were compared with the theoretical model, the generalized two-center cluster model (GTCM) with the $\alpha + \alpha + 4n$ configuration [22–26]. The resonance sequence and the decay width in the theoretical calculation are completely consistent to the experimental observations [22,23]. Furthermore, the observed decay scheme into different channels, such as $^{12}\text{Be} \rightarrow \alpha + {}^8\text{He}$ and $^6\text{He} + {}^6\text{He}$, is also consistent with the GTCM calculation [24,25].

Excited states having the characteristic intrinsic structures are usually observed as intermediate resonances with a width of $\Gamma_R \leqslant 1$ MeV above a particle decay threshold, and the determination of their resonance parameters, such as the resonance energy and the decay width, is essential in the quantitative analyses of the intrinsic structure of the intermediate resonances. In determining the resonance parameters, the evaluation of the nonresonant background strength, which has a broad continuum structure, is indispensable. The background strength is expected to be generated by a one-step transition from the initial ground state to the final state, which corresponds to the scattering continuum state with the effect of the final state interaction (FSI) among the decaying particles. However, the breakup strength is often evaluated without FSI [5], and there is no systematic formula to evaluate the nonresonant background strength with a strong FSI.

In this article, we propose a new formula to evaluate the background strength for the binary breakup reaction with FSI by extending the Migdal-Watson (MW) formula [27–29]. This formula was originally valid for the s-wave breakup in binary systems composed of the charge neutral particles, and the strength is parametrized in terms of two variables in the effective range theory: the scattering length and the effective range [30]. Here we try to generalize the MW formula by introducing extra parameters to describe the nonresonant background in the general binary breakup reactions. The preliminarily result of our extended formula was published in Ref. [31]. Although the sophisticated calculations for the breakup reactions have largely progressed [18–21], a simple formula to evaluate the background contribution is still unestablished. Thus, the development of a simple formula to describe the background strength is quite constructive for the pragmatic analyses of experimental data.

In the evaluations of the nonresonant background strength generated by the binary breakup, we employ the complex scaling method (CSM) [32], which is a powerful tool to describe few-body continuum states. We check the validity of the extended MW formula by fitting the nonresonant background strength evaluated from the CSM calculation. In the present analysis, we consider the breakup of ^{20}Ne into $\alpha + {}^{16}\text{O}$ because the ^{20}Ne nucleus is known to be a typical example of a binary cluster system, and the $\alpha + {}^{16}\text{O}$ cluster model nicely reproduces the observed energy spectra in ^{20}Ne [33]. A similar calculation is applied to the breakup of $^{12}\text{Be} \rightarrow \alpha + {}^8\text{He}$ [10].

The organization of this article is the following. In Sec. II, theoretical formulation is explained. The original Migdal-Watson theory and its extension are explained in Sec. III. In Sec. IV, the computational results are shown, and the validity of the extended MW formula is discussed. The final section is devoted to a summary.

II. THEORETICAL FRAMEWORK

In the present calculation, the complex scaling method (CSM) is a basic computational procedure of the nonresonant breakup process going to binary fragments. The details of the theoretical framework are given in Ref. [32]. We briefly explain the essence of the present calculation in the following.

A. Complex scaling method

In the complex scaling method (CSM) [32], the transformation of the complex rotation with the rotation angle θ,

$$\hat{U}(\theta)f(\mathbf{r}) = e^{\frac{3}{2}i\theta}f(e^{i\theta}\mathbf{r}) = f^{\theta}, \tag{1}$$

is introduced for the arbitrary function of $f(\mathbf{r})$. Here the rotation on $\mathbf{r}$ should be read as the transformation on the radial part of the coordinate, hence $r \rightarrow re^{i\theta}$. The Schrödinger equation transformed by this complex rotation becomes

$$\hat{H}^{\theta}\Psi^{\theta} = E^{\theta}\Psi^{\theta}, \tag{2}$$

where Ψ^{θ} is defined by Eq. (1) and $\hat{H}^{\theta} = \hat{U}(\theta)\hat{H}\hat{U}(\theta)^{-1}$. In the rotated Hamiltonian $\hat{H}^{\theta}$, the dynamical coordinates of $\mathbf{r}$ contained in $\hat{H}$ are complex rotated: $\hat{H}^{\theta} = \hat{H}(e^{i\theta}\mathbf{r})$. The amplitude of the resonant wave function, which originally diverges in the asymptotic region, is damped in the large-distance region by this complex rotation, hence the usual computation technique for the bound state problem, the basis expansion method, is applicable. The energy eigenvalues calculated from CSM plus the basis expansion technique becomes the discrete and complex eigenvalue $E^{\theta} \rightarrow E_{\nu}^{\theta}$ labeled by the eigenvalue number ν. According to the ABC (Aguilar, Combes and Balslev) theorem [32], the energy eigenvalues for the bound state are invariant, and the eigenvalues for the resonances are clearly separated from the nonresonant continuum states in the complex energy plane [32].

The CSM is applicable to the calculation of the strength function, which represents the transition strength of the initial ground state (Ψ_i) induced by the external field $\hat{O}_{\lambda}$ with the multipolarity λ [34]. The definition of the strength function $S_{\lambda}(E)$ is given by

$$S_{\lambda}(E) = \sum_f |\langle\Psi_f|\hat{O}_{\lambda}|\Psi_i\rangle|^2\delta(E - E_f), \tag{3}$$

where Ψ_f denotes the final state belonging to the fth eigenstate excited by the external field $\hat{O}_{\lambda}$. By introducing the complex rotation given by Eq. (1) and the extended completeness relation [32,34], the strength function is rewritten as

$$S_{\lambda}(E) = -\frac{1}{\pi} \operatorname{Im} R_{\lambda}(E) \tag{4}$$

with the response function of $R_\lambda(E)$ defined by

$$R_\lambda(E) = \sum_\nu \frac{\langle \tilde{\Psi}_i^\theta | (\hat{O}_\lambda^\dagger)^\theta | \Psi_\nu^\theta \rangle \langle \tilde{\Psi}_\nu^\theta | \hat{O}_\lambda^\theta | \Psi_i^\theta \rangle}{E - E_\nu^\theta}. \tag{5}$$

Here Ψ^θ is the solution of CSM, and the tilde in the bra state means that the complex conjugate is not taken for the radial part of the wave function [32]. Equations (4) and (5) are derived in Eqs. (2.1) and (2.8) in Ref. [34].

B. Operators for direct breakup

In the present calculation, we assume that the nonresonant breakup of the binary system occurs in the one-step transition, which is often called the direct breakup. The direct breakup is simulated by the strength and response functions in CSM, shown in Eqs. (4) and (5). Equation (5) represents the response function of a nucleus, which describes the decay process under the external field $\hat{O}_\lambda$. In the strict meaning, the response function is different from the transition matrix in a realistic breakup reaction, in which the nucleus is dissociated by the nuclear interaction from other nucleus. However, the transition matrix for the breakup can be reduced to the response function with a multipole operator proportional to the spherical harmonics if we assume a one-step transition for the breakup process under the plane wave approximation with the zero-range nuclear interaction between the colliding nuclei, as shown in a series of equations of Sec.14.1.2 in Ref. [35]. A detailed explanation about the relation of the response function and the transition matrix is also shown in Ref. [27].

The resultant operator in the one-step breakup process is derived in Eq. (14.10) in Ref. [35], and it has the form

$$\hat{O}_\lambda \sim \sum_i j_\lambda(Q r_i) Y_{\lambda\mu}(\hat{r}_i), \tag{6}$$

which is written in terms of the nucleon coordinate $\boldsymbol{r}_i$ with a nucleon number i in the breakup nucleus. Here j_λ and $Y_{\lambda\mu}$ represent the spherical Bessel function and the spherical harmonics, respectively, and the former contains the momentum transfer Q. The expansion in j_λ over Q generates a series of operators having the functional form of the power of r_i multiplied by $Y_{\lambda\mu}$.

The operator in Eq. (6) is expressed in terms of the nucleon coordinates $\boldsymbol{r}_i$, but a specific part of the operator depending on the relative coordinate $\boldsymbol{R}$ between the breakup fragments can be extracted by introducing coordinate rearrangement [3,36,37]. In the final expression, we can obtain the standard operator with multipolarities of $\lambda = 1$ and 2 as the external field inducing the direct breakup in the binary system:

$$\hat{O}_\lambda = \sqrt{4\pi} R^\lambda Y_{\lambda,0}(\hat{\mathbf{R}}), \quad \lambda = 1, 2, \tag{7}$$

where $\mathbf{R}$ denotes the relative coordinate of two fragments. The derivations of these monopole and quadrupole operators can be confirmed in Eqs. (4) and (6) in Ref. [36], respectively. In addition, the higher-order operators are also generated from the momentum expansion in j_λ, and we consider such

higher order operators for the monopole and dipole excitations, which are given by

$$\hat{O}_{\lambda=0} = \sqrt{4\pi} R^2 Y_{0,0}(\hat{\mathbf{R}}), \tag{8}$$

$$\hat{O}_{\lambda=1} = \sqrt{4\pi} R^3 Y_{1,0}(\hat{\mathbf{R}}). \tag{9}$$

The explicit derivation of the monopole operator is shown in Eq. (2.15) in Ref. [3], while that of the dipole operator can be seen in Eq. (12) in Ref. [37]. The importance of the cluster excitation by these higher order operators has recently been pointed out in Refs. [3,4,37,38].

A special treatment is required in the calculation of the monopole transition using Eq. (8). In the matrix element for the response function in Eq. (5), the operation of the monopole operator ($\hat{O}_{\lambda=0}$) on the initial wave function (Ψ_i) in the ground state generates the superposition of a series of wave functions, which contains both the ground and excited states. Thus, the ground state component must be extracted from the product of the monopole operator and the initial wave function, which is called the initial wave packet [27]. This exclusion can be achieved by the replacement in the radial operator $R^2 \to R^2 - \langle R^2 \rangle$, in which $\langle R^2 \rangle$ denotes the expectation value of R^2 with the ground wave function.

C. Interaction potentials and wave functions

In the calculation of the $\alpha + {}^{16}$O system, the computational setting is basically same as those in Ref. [33]. The interaction potential V, which is used to calculate the initial and final wave functions, is composed of the nuclear (V_N) and Coulomb (V_C) potentials, and their explicit form is given by

$$V(R) = V_N(R) + V_C(R), \tag{10}$$

$$V_N(R) = -154 \exp(-0.1102 R^2), \tag{11}$$

$$V_C(R) = 16 \frac{e^2}{R} \operatorname{erf}(0.4805 R), \tag{12}$$

with the definition of the error function being

$$\operatorname{erf}(x) = \frac{2}{\sqrt{\pi}} \int_0^x \exp(-t^2) dt. \tag{13}$$

The energy levels calculated from these potentials can reproduce the experimental spectra of the ground and excited rotational bands, which correspond to the parity doublet in the $\alpha + {}^{16}$O configuration [33].

In the calculation of $\alpha + {}^8$He, we construct the nuclear potential [$V_N(R)$] by the double folding (DF) procedure [39], which is symbolically written as a function of the α-^{8}He relative coordinate, $\mathbf{R}$:

$$V_N^{\mathrm{DF}}(R) = \iint \rho_\alpha(\mathbf{r}_\alpha) \rho_8(\mathbf{r}_8) \times v_{\mathrm{NN}}^{\mathrm{DDM3Y}}(s, \rho) d\mathbf{r}_1 d\mathbf{r}_2 \tag{14}$$

with $s = |\mathbf{r}_8 - \mathbf{r}_\alpha - \mathbf{R}|$. Here $\mathbf{r}_\alpha$ ($\mathbf{r}_8$) denotes a coordinate measured from the center of mass in the α particle (^{8}He).

The densities of the α particle (ρ_α) and ^{8}He (ρ_8) assuming the lowest shell model configurations [$(0s)^4$ and $(0s)^4(0p)^4$] are constructed to reproduce the charge form

factor of the electron scattering and the observed nuclear radius, respectively. In Eq. (14), v_{NN}^{DDM3Y} represents the effective nucleon-nucleon (NN) interaction, which acts between a pair of nucleons contained in α and ^{8}He. In the present calculation, we adopt the DDM3Y (density-dependent Michigan three-range Yukawa) interaction [39,40]. The Coulomb potential (V_C) is generated by an error function similar to Eq. (12).

The DF potential with DDM3Y has been successful in various applications to scattering problems from the low-energy molecular resonance region [41–43] to the high energy region [44,45]. The successful applications of DDM3Y mean that the asymptotic behavior of the wave function for the scattering particles is precisely described by this potential because the cross section is sensitive to the outer part of the scattering wave function. Since the response function in Eq. (5) is also sensitive to the outer parts of the wave function in the initial bound state (Ψ_i), we can consider that the DF potential with DDM3Y is a realistic nuclear potential for handling the response function.

The computational condition to prepare the initial wave function (Ψ_i) and the final one (Ψ_f) for the α-^{16}O relative motion is basically the same as that in Ref. [33]. Namely, the pseudopotential with the harmonic oscillator wave function is included to exclude the Pauli forbidden states in solving the Schrödinger equation in addition to the potentials shown in Eqs. (10), (11), and (12) [33,34].

In the case of $\alpha + ^8$He, the DF potential in Eq. (14) and the Coulomb potential with the error function are used in solving the wave functions of the α-^{8}He relative motion, and we do not include the pseudopotential. Instead of the pseudopotential, we consider the Wildermuth condition to take into account the Pauli exclusion principle between two He nuclei for simplicity [46]. When we assume the lowest shell model configurations of $(0s)^4$ and $(0s)^4(0p)^4$ for α and ^{8}He, respectively, the total oscillator quanta (N) for the lowest allowed state is $N = 4$ for the $\alpha + ^8$He configurations.

III. MIGDAL-WATSON THEORY AND ITS EXTENSION

A. Migdal-Watson theory for the strength function

In the s-wave breakup of a binary system composed of charge neutral particles, the strength function can be expressed by a closed formula in the case of the short range limit of spatial size in the initial wave function. This formula was originally developed by Migdal and Watson, and it is called the Migdal-Watson (MW) theory [28,29]. This formula expresses the strength function in terms of two parameters in the effective range theory [30]. A detailed explanation of the MW formula is reported in Ref. [27]. Here we briefly explain the MW formula in the following.

If the final state wave functions of Ψ_f are not the discrete state but the continuous distorted wave specified by the asymptotic momentum **k** with the relation of the decay energy $E(\mathbf{k}) = \hbar^2 k^2/2m$, the completeness relation of $\sum_f |\Psi_f\rangle\langle\Psi_f| = \sum_f |E_f\rangle\langle E_f| = 1$ is replaced by $\int d\mathbf{k}|\mathbf{k}\rangle\langle\mathbf{k}| = 1$, and the strength function in Eq. (3) for the direct breakup going to the binary continuum state becomes

$$S_\lambda(E)dE \propto \left|\langle\chi_{k,\lambda}^{(f)}|\hat{O}_\lambda|\chi^{(i)}\rangle\right|^2 k^2 dk. \tag{15}$$

In this expression, $\chi^{(f)}(\mathbf{R})$ and $\chi^{(i)}(\mathbf{R})$ represent the final and initial wave functions for the relative motion of the binary system. When we consider the s-wave state for the initial wave function $[\chi^{(i)}(\mathbf{R}) = \chi^{(i)}(R)]$, the final wave function has a definite relative spin, which is the same as the multipolarity (λ) in the operator $\hat{O}_\lambda$. In Eq. (15), the distorted wave in the final state is specified by the magnitude of the momentum of k, and the angular part of the asymptotic momentum ($\hat{\mathbf{k}}$) is dropped by the angular integration in the completeness relation.

We express the distorted wave in the reduced form

$$\chi_{k,\lambda}^{(f)}(\mathbf{R}) = \frac{w_{k,\lambda}(R)}{kR}Y_\lambda(\hat{\mathbf{R}}) \tag{16}$$

and consider the monopole transition, $\lambda = 0$, which corresponds to the s-wave scattering state in the final state. In the $k \to 0$ limit of the s-wave scattering without Coulomb interaction, we can use the effective range theory [30]. According to this theory, the wave function $\omega_{k,\lambda=0}(R)$ inside of the nuclear potential is almost independent of both of the collision energy and the details in the potential shape if the depth of the nuclear potential is much larger than the collision energy. In this situation, it is possible to use the approximated relation $w_{k,0}(R) \sim \xi(R)\sin\delta_k$ with the s-wave phase shift δ_k and the fixed radial function of $\xi(R)$. This approximation is valid inside of the nuclear interaction.

We call the product of the initial wave function and the operator, such as $\hat{O}_{\lambda=0}\chi^{(i)}$ in Eq. (15), the initial wave packet. If the initial wave packet is strongly confined inside of the nuclear interaction, we can obtain the energy dependence of $\sin^2\delta_k$ in the strength function, such as

$$S_0(E)dE \propto \frac{\sin^2\delta_k}{k}dE, \tag{17}$$

by employing the relation $w_{k,0}(R) = \xi(R)\sin\delta_k$ in Eqs. (15) and (16). This expression using $\sin\delta_k$ is called the Migdal-Watson (MW) approximation [28,29]. The details of the MW approximation are explained in Eq. (73) in Ref. [27]. Furthermore, by using the well known relation

$$k\cot\delta_k \sim -\frac{1}{a_{sc}} + \frac{r_0}{2}k^2 \tag{18}$$

with the scattering length a_{sc} and the effective range r_0, we obtain the final expression of

$$S_0(E)dE \propto \frac{k}{k^2 + \left(\frac{1}{a_{sc}} - \frac{r_0}{2}k^2\right)^2}dE$$

$$= \frac{\sqrt{E}}{AE^2 + BE + C}dE, \tag{19}$$

where the constants A, B, and C are functions of a_{sc} and r_0. The MW formula in Eq. (19) is valid for the breakup from the initial wave packet strongly localized inside of the nuclear interaction because we use the relation $w_{k,0}(R) = \xi(R)\sin\delta_k$, which holds only in the spatial range of the nuclear interaction, in the whole region of the integration in Eq. (15).

The final expression in Eq. (19) has a peak in the variation of the energy, which is determined by the quadratic energy

denominator, and the peak structure depends on the functional form in the numerator, $\sqrt{E}$, which corresponds to the phase volume for the decaying particles. Due to these two factors, the strength function starts from zero at $E = 0$ (threshold energy for the binary decay) and goes to zero at $E \to \infty$. The former behavior is due to the increase of the phase volume, while the latter is generated by the higher nodal behavior in the final scattering state, which cancels the integration in the matrix elements contained in Eq. (15). Thus, a single and broad peak must appear in the energy distribution of the strength function as long as there are no special intrinsic structures in the final and initial wave functions. This is a general feature in the structureless strength function generated by the direct (one-step) breakup, and we should keep in mind this basic feature when extending the MW formula in Eq. (19).

B. Extension of Migdal-Watson theory

The MW formula shown in Eq. (19) is valid for the s-wave breakup from the initial wave packet localized inside of the nuclear interaction, which corresponds to the tightly bound system composed of the charge neutral fragments. Here we try to extend Eq. (19) to describe the direct breakup reaction of general binary systems, which have finite charge, finite spin in the final scattering state ($\lambda \neq 0$), and finite size of the initial wave packet. Since the basic feature of the single peak structure confirmed in Eq. (19) should be invariant, in the present extension, it is quite natural to consider the functional form

$$S_\lambda(E) \propto \frac{f_\lambda(E)}{(AE^2 + BE + C)}, \tag{20}$$

where the function $f_\lambda(E)$ represents the modification function for $\sqrt{E}$ appearing in the original MW formula. We include all of the finite effects in this modification function.

First, we consider the correction arising from the final distorted wave to take into account the effects of the finite charge and the finite spin. One naive choice to take into account these effects is to set $f_\lambda(E)$ to the penetration factor $P_\lambda(ka)$ with the channel radius a, because the penetration factor with the limit of $k \to 0$ is reduced to the phase volume, $\sqrt{E}$, in the case where the final scattering states are the charge neutral and $\lambda = 0$ states.

We can justify the introduction of the penetration factor $P_\lambda(ka)$ by the plane wave approximation for the final distorted wave in Eq. (15). The plane wave approximation of Eq. (15) with the multipolarity λ becomes

$$S_\lambda(E)dE \propto |\langle j_{\lambda,k} Y_\lambda | \hat{O}_\lambda | \chi^{(i)} \rangle|^2 k \, dE, \tag{21}$$

where $j_{\lambda,k}$ denotes the spherical Bessel function with the rank λ and the momentum k. If the initial wave packet is strongly localized inside of the small radius a, we can obtain the following expression by taking the limit of $k \to 0$:

$$S_\lambda(E)dE \propto (ka)^{2\lambda+1} |\langle Y_\lambda | \hat{O}_\lambda | \chi^{(i)} \rangle|^2 dE, \tag{22}$$

where we use the relation of $j_{\lambda,k} \to j_\lambda(kR)|_{R=a} \sim (ka)^\lambda$ by replacing the radial coordinate R with the radius a. A factor of $(ka)^{2\lambda+1}$ in Eq. (22) is the same as the penetration factor of

$P_\lambda(ka)$ for the low energy limit ($k \to 0$) in the decays of the charge neutral particles.

Second, the effect of the finite size (or the finite binding energy) for the initial wave packet is considered. If two constituent particles in the ground state are described by the shell model with the harmonic oscillator (HO) potential, the relative wave function of the two particles [$\chi^{(i)}(R)$ in Eq. (21)] is also described by the HO wave function ($\chi_{HO}^{(i)}$). The asymptotic behavior in the HO relative wave function is determined by an exponential function, such as $\chi_{HO}^{(i)}(R) \sim \exp(-\nu R^2)$ with the parameter of $\nu = \mu/2b^2$, in which μ and b represent the reduced mass number of the binary system and the width parameter of the HO potential, respectively.

The strength function is reduced to the Fourier transformation of the initial wave packet in the plane wave approximation of Eq. (21), hence it corresponds to the Fourier transformation of the HO wave packet, which is the HO wave function multiplied by the external operator, $\hat{O}_\lambda \chi_{HO}^{(i)}$. Since the radial part in the external field is given by the power of the radial coordinate, the Fourier component with the momentum k in the initial HO wave packet must have the functional form $\exp(-b^2 k^2 / 2\mu)$. Therefore, it is valid to include the factor $\exp(-\beta E)$ in the energy dependence of the breakup strength, where the parameter β is sensitive to the spatial size of the initial wave packet.

After summarizing the above consideration, the most probable candidate for the analytic function to describe the background strength due to the direct breakup will be

$$S_\lambda(E) \propto \frac{P_\lambda(ka)e^{-\beta E}}{AE^2 + BE + C}. \tag{23}$$

$P_\lambda(ka)$ is a monotonically increasing function in energy, and its rising position is controlled by the channel radius a, while the three parameters (A, B, C) in the quadratic energy denominator determine the peak energy and the distribution width. In contrast, β in the exponential term controls the damping behavior in the high energy region. Two parameters are newly introduced, β and a, which are sensitive to the spatial size of the initial wave packet, but these parameters do not change the basic feature in the structureless strength function expected from the original MW formula in Eq. (19).

It is instructive to reconsider the extended formula in Eq. (23) in connection to the effective range theory. $e^{-\beta E}$ is introduced to take into account the finite size of the initial bound state, while $P_\lambda(ka)$ and $(AE^2 + BE + C)^{-1}$ reflect the feature in the final scattering state. Therefore, A, B, C, and a must have a certain relation to the parameters in the effective range theory: the scattering length a_{sc} and the effective range r_0. A, B, and C are directly connected to (a_{sc}, r_0) through Eq. (18), which is valid for the s-wave scattering in a charge neutral system, but this relation is no longer applicable in scattering with finite angular momentum and finite Coulomb potential [47]. On the other hand, the channel radius a, which appears when extending the phase factor $\sqrt{E}$, was not originally included in the effective range theory [30,47].

In scattering with finite angular momentum under a finite Coulomb potential, the relation of the phase shift and (a_{sc}, r_0) becomes a nonlinear equation using the Sommerfeld parameter as shown in Eq. (21) in Ref. [47]. Furthermore, we need

to employ the *R*-matrix formalism for the density of state to establish the close relation of the channel radius *a* and the phase shift as shown in Ref. [48]. Therefore, it is not so easy to establish the explicit relation of (A, B, C, a) and (a_{sc}, r_0) in the case of finite angular momentum and finite Coulomb potential. In the formulation of Eq. (23), the set of parameters should be handled as phenomenological parameters, which are independent of (a_{sc}, r_0), to determine the low energy part of the strength function.

IV. RESULTS

In this section, we discuss the applicability of the extended MW formula in Eq. (23) by comparing with the direct breakup evaluated by the CSM calculation. First, we calculate the direct breakup of ^{20}Ne $\rightarrow \alpha + ^{16}$O, and the breakup strength is compared with the extended MW formula in Eq. (23). Second, we demonstrate that newly introduced parameters β and a are really sensitive to the spatial size of the initial wave packet. Finally, the extended MW formula is applied to the direct breakup of ^{12}Be $\rightarrow \alpha + ^8$He.

A. Analysis of ^{20}Ne $\rightarrow \alpha + ^{16}$O

We have solved the complex-scaled Schrödinger equation in Eq. (2) with the $\alpha + ^{16}$O model in ^{20}Ne, which is a similar calculation to the CSM calculation in Ref. [33], and the wave functions of the initial bound state (Ψ_i) and final continuum states (Ψ_f) are prepared. This binary model reproduces the binding energy of the α particle ($E_B \approx -4.7$ MeV), and the calculated spectra of the ground and excited rotational bands reproduce the experimental observation.

The CSM strength function for one-step direct breakup is calculated according to the expression in Eqs. (4) and (5) [34]. The computational results of the CSM strength function and the fitting by the extended MW formula in Eq. (23) are shown in the two panels of Fig. 1. The quadrupole and monopole strengths for ^{20}Ne $\rightarrow \alpha + ^{16}$O are shown in the top and bottom panels, respectively. The CSM strengths shown by the solid curve with the dots are nicely reproduced by the extended MW formula plotted by the open circles. In these strength functions, there are the broad peaks, which is consistent with the basic feature in the structureless strength, hence the calculated CSM strength fitted by the extended MW formula is considered to appropriately describe the nonresonant background in a binary breakup reaction.

In both panels, the open square and the error bar represent the real and imaginary parts of the energy pole, respectively, giving the zero value in the denominator of the response function in Eq. (5). Since the final state interaction (FSI) in the $\alpha + ^{16}$O scattering state, such as the nuclear + Coulomb + centrifugal potentials, is fully taken into account, the energy pole is generated by FSI in the final scattering state after the breakup. The strength function evaluated by CSM has a broad continuum distribution consistent with the feature of the structureless background, and this enhancement is basically generated by the competition of the increase of the phase volume and the decrease of the matrix element as a function of energy. However, the energy pole created by FSI also
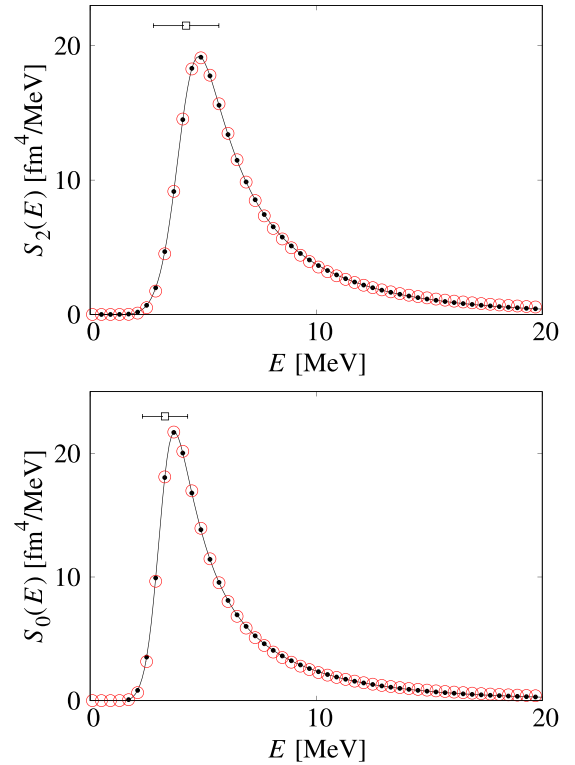
FIG. 1. Comparison of the strength function of ^{20}Ne $\rightarrow \alpha + ^{16}$O with fitting results by the extended Migdal-Watson formula in Eq. (23). The top panel shows the quadrupole [$S_2(E)$] transition, while the bottom one shows the monopole [$S_0(E)$] transition. The α threshold energy is set to the zero point in the abscissa. In both panels, the dots connected by the solid curve and open circles represent the strength function calculated from CSM and fitting results using Eq. (23), respectively. The open square and the error bar correspond to the real and imaginary parts of the energy pole appearing in the response function in Eq. (5), respectively. Similar figures are also shown in Ref. [31].

contributes to the enhancement in the strength function if the strong FSI is effective between the scattering particles.

In the fitting analysis of the quadrupole transition, we use the parameters for the energy denominator part: $A = 0.025$, $B = -0.21$, $C = 0.48$, $a = 5.5$ fm, and $\beta = 0.015$ MeV^{-1} in Eq. (23). In the monopole transition, the parameters used for the fitting to the monopole transition are $A = 0.029$, $B = -0.19$, $C = 0.33$, $a = 5.0$ fm, and $\beta = 0.015$ MeV^{-1}.

In order to reproduce the peak structures shown in Fig. 1, the fitting only by the quadratic energy denominator in Eq. (23) is insufficient, and some sort of a modification function $f_\lambda(E)$ is clearly needed. Here we have tried to reproduce the strength by considering only a penetration factor like $f_\lambda(E) = P_\lambda(ka)$. The results with and without $e^{-\beta E}$ are compared in Fig. 2. In this figure, the strength of the quadrupole transition [$S_2(E)$, shown in the top panel of Fig. 1] is plotted. The deviation of the fitting result by the extended MW formula with finite β (open circles) from the CSM strength (solid curve) is small but the fitting with $\beta = 0$ (dashed curve) overestimates the CSM strength in the higher energy region. The deviation from the CSM result seems not to be large
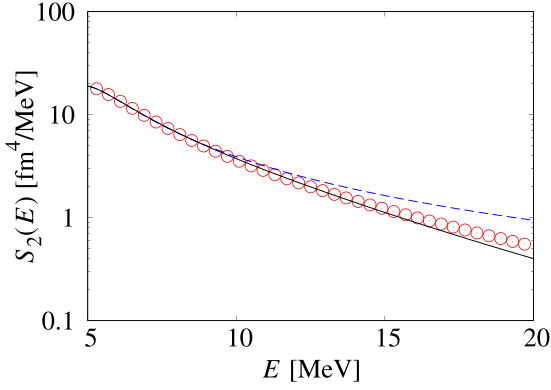
FIG. 2. Logarithmic plot of the strength function of quadrupole transition in $\alpha + {}^{16}$O. The solid curve and open circles represent the CSM strength and the fitted results by the extended MW formula, while the dotted curve shows the fitting result without the exponential damping function, $e^{-\beta E}$. The solid curve and the open circles are the same as the solid curve with the dots and the open circles, respectively, in the top panel in Fig. 1.

but we have confirmed that this deviation becomes prominent in strength for higher multipolarity. Thus, the exponential damping function is important to reproduce the strength in the higher energy region.

B. Spatial size of initial wave packet and fitting parameters

The extra parameters, such as β and a, are introduced in the extension of the MW formula. We demonstrate that these newly introduced parameters have a close relation to the spatial size of the initial wave packet by controlling the binding energy of the initial wave function. In Fig. 3, the radial part of the initial wave packets, $\hat{O}_{\lambda=2}(\mathbf{R})\chi^{(i)}(R) \rightarrow R^2\chi^{(i)}(R)$, and the respective strength functions for the quadrupole transition in ^{20}Ne $\rightarrow \alpha + {}^{16}$O are shown in the top and bottom panels, respectively.

In the top panel, the dashed, dotted and solid curves show wave packets with binding energies of $E_B = -8.29, -4.64$, and -1.40 MeV, respectively. The initial wave packet is more extended as the binding energy gets shallower in the top panel. In the bottom panels, the strength functions corresponding to the wave packets in the top panel are shown; the curves labeled by $-8.29, -4.64$, and -1.40 MeV in the bottom panel correspond to the dashed, dotted, and solid curves in the top panel, respectively. As the spatial size of the initial wave packet is extended, the corresponding strength function is more shrunken. This behavior basically originates from a feature of the Fourier transformation involved in the strength function.

The open circles in the bottom panel show the results using the extended MW formula in Eq. (23) with the appropriate values of β. The fitting results by the extended MW formula nicely reproduce the strength functions calculated for the various sizes of the initial wave packets. As the system becomes a weakly bound state having a spatially extended wave function, the parameter β becomes large: $(E_B, \beta) = (-8.29, 0.0015) \rightarrow$
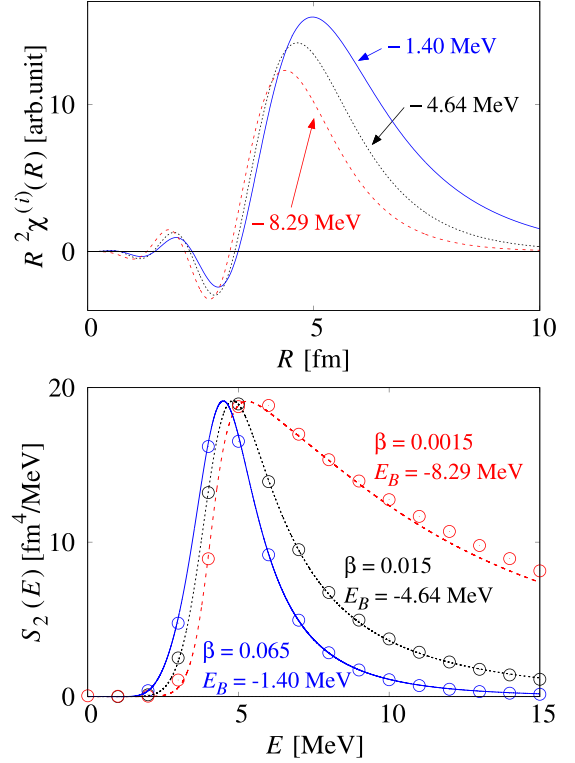
FIG. 3. Size and binding energy dependence of initial wave packets and strength functions in $\alpha + {}^{16}$O system. In the top panel, the initial wave packets calculated at the binding energies of $E_B = -8.29$ MeV (dashed curve), -4.64 MeV (dotted curve), and -1.40 MeV (solid cuve) are shown, while the respective strength functions are shown in the bottom panel. The binding energies attached to the individual curves in the bottom panel correspond to the wave packet labeled by the respective binding energies in the top panel. In the bottom panel, the open circles show the fitting results by the extended MW formula, and the parameters of β used in the fitting are attached to the individual sets of open circles.

$(-4.64, 0.015) \rightarrow (-1.40, 0.065)$. Thus, the parameter β has a close connection to the spatial size of the initial wave packet.

In order to understand the relation of the spatial size of the initial wave packet and β more deeply, we calculate several strength functions by varying the binding energies and tried to find the optimal β in Eq. (23). In Fig. 4, several root-mean-squared radii of the initial wave function (open circles), $\sqrt{\langle R^2 \rangle} \equiv \sqrt{\langle \chi^{(i)} | R^2 | \chi^{(i)} \rangle}$, are plotted as a function of the fitting parameter β. Here $\sqrt{\langle R^2 \rangle}$ and β are derived from the quadrupole transition in ^{20}Ne $\rightarrow \alpha + {}^{16}$O. In this figure, we can clearly confirm the positive correlation in the plot of $\beta - \sqrt{\langle R^2 \rangle}$; larger $\sqrt{\langle R^2 \rangle}$ (weak binding) requires more enhanced β (shrunken strength function). Therefore, the parameter β correlates to the spatial size of the initial wave function or the initial wave packet, which is given by the initial wave function multiplied by the external operator.

In Fig. 4, the solid curve shows the fitting curve for the calculated data points (open circles), and its functional form is given by $\sqrt{\langle R^2 \rangle} = 5.0\sqrt{\beta} + 3.5$. We can easily understand that the root-mean-squared radius $\sqrt{\langle R^2 \rangle}$ is proportional to
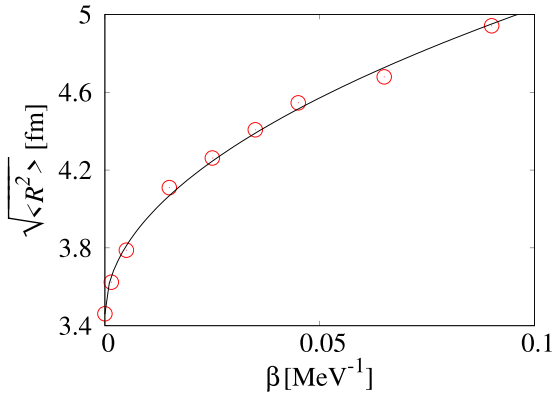
FIG. 4. Root-mean-squared radii ($\sqrt{\langle R^2 \rangle}$) of the initial wave function of $\chi^{(i)}(R)$ plotted as a function of the fitting parameter β in Eq. (23), which is derived from the quadrupole transition in ^{20}Ne $\rightarrow \alpha + ^{16}$O. The open circles show the result of the analysis by Eq. (23), while the solid curve shows the fitting function of the open circles, which is given by $\sqrt{\langle R^2 \rangle} = 5.0\sqrt{\beta} + 3.5$.

$\sqrt{\beta}$ by employing the HO model. If we assume the initial wave function to be the pure HO wave function, we can obtain the following relation from the Virial theorem:

$$\sqrt{\langle R^2 \rangle} = \sqrt{\frac{\hbar^2}{\mu m}\left(N + \frac{3}{2}\right)}\sqrt{\beta}, \qquad (24)$$

where μ and m represent the reduced mass number of the binary channel and the nucleon mass, respectively. In the pure HO model, β is given by $m(b/\hbar)^2$. N in the parentheses means the total oscillator quantum number, which has the relation $N = 2n + L$ with the number of the radial node n and the relative spin L of the initial wave function in the binary system. If we evaluate Eq. (24) for the $\alpha + ^{16}$O system with the lowest allowed quanta, $N = 4$, we obtain $\sqrt{\langle R^2 \rangle} = 11.1\sqrt{\beta}$, which deviates considerably from the fitting result of $\sqrt{\langle R^2 \rangle} \sim 5.0\sqrt{\beta}$. Although the fitting result of the channel radius a is not shown, we have found a similar positive correlation in the plot of $a - \sqrt{\langle R^2 \rangle}$ because the channel radius a also has a direct relation to the spatial size of the initial wave packet as shown in the plane wave approximation of Eqs. (21) and (22).

C. Application to ^{12}Be $\rightarrow \alpha + ^8$He

Finally, we apply the extended MW formula to the breakup of ^{12}Be into $\alpha + ^8$He, in which prominent resonances are observed in experiments [8–12]. Here we calculate the direct breakup from the bound state to the scattering continuum in the $\alpha + ^8$He$_{g.s.}$ system.

In the two panels of Fig. 5, the calculated strength functions are compared with the fitting analysis by the extended MW formula in Eq. (23). The top and bottom panels represent the quadrupole [$S_2(E)$] and monopole [$S_0(E)$] strengths, respectively. The strength function rapidly increases in the lower energy region of $E < 1$ MeV because of the weakness of the Coulomb potential in comparison to that in the $\alpha + ^{16}$O system. The calculated strength functions (dots connected by
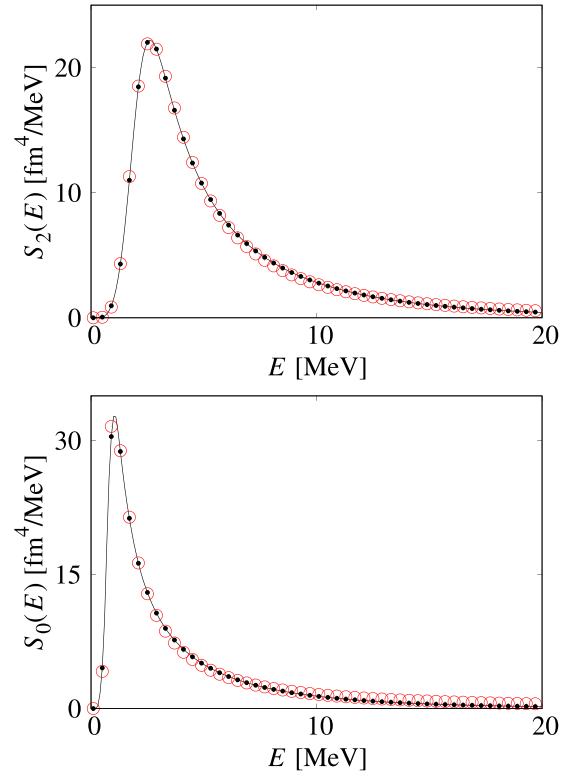
FIG. 5. Strength functions for direct breakup of ^{12}Be $\rightarrow \alpha + ^8$He. The top and bottom panels show the quadrupole [$S_2(E)$] and monopole [$S_0(E)$] transitions, respectively. The calculated strength functions are plotted by the solid curve with the dots, while the results of the fitting functions in Eq. (23) are drawn by the open circles. α threshold energy is set to zero in the abscissa.

solid curves) with the single peak structure are nicely reproduced by the fitting function (open circles).

Similar calculations for the dipole excitations are shown in Fig. 6. In the top panel, the result for the normal dipole excitation induced by the operator of $RY_{1,0}(\hat{\mathbf{R}})$ is shown, while the result of a higher order dipole operator, $R^3Y_{1,0}(\hat{\mathbf{R}})$, is plotted in the bottom panel. The calculated strength function (solid curve with dots) has a single peak structure, and it is almost the same as the fitting result (open circles) using the extended MW formula.

We have checked the strength function with higher multi-polarity, such as the octupole [$R^3Y_{3,0}(\hat{\mathbf{R}})$] and hexadecapole [$R^4Y_{4,0}(\hat{\mathbf{R}})$] transitions, and found that the proposed formula in Eq. (23) reproduces the calculated strength function fairly well. All of the reproductions shown in Figs. 5 and 6 are achieved only by the combination of the penetration factor $P_\lambda(ka)$ and the exponential term $e^{-\beta E}$ in Eq. (23), and the restricted fit without the exponential term overestimates the strength in the higher energy region.

V. SUMMARY

In summary, we have developed a simple formula to describe the non-resonant background strength generated by direct breakup in binary systems, in which the final state
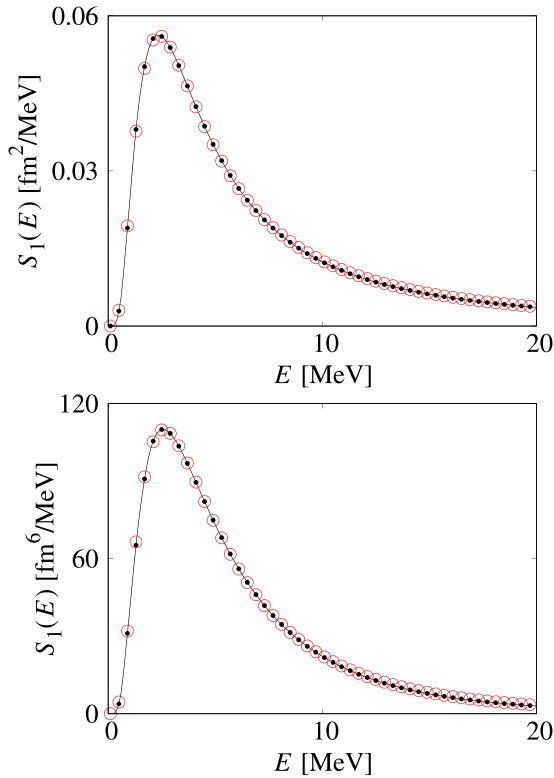
FIG. 6. Same as Fig. 5 except for the normal and higher dipole operators. The top and bottom panels show the transition by the operator $RY_{1,0}(\hat{\mathbf{R}})$ and the dipole operator $R^3Y_{1,0}(\hat{\mathbf{R}})$, respectively.

interaction between the decaying particles is taken into account. The direct breakup process is assumed to be a one-step transition from the binary bound state to its scattering state. The transition strength of the direct breakup can be reduced to the response function of a single nucleus, and the direct breakup is considered to be the main component of the nonresonant background strength in a realistic breakup experiment. The evaluation of the background strength is very important in deriving the resonance parameters from the total strength observed in experiments.

In order to describe the background strength in a simple manner, we have considered an analytic function by extending the Migdal-Watson (MW) formula [28–30], which has recently been discussed in connection with the s-wave breakup of a dineutron system [27]. In the original MW formula, a simple function in energy, such as $\sqrt{E}/(AE^2 + BE + C)$, is derived by employing the effective range theory [30]. This formula is valid for the s-wave binary breakup of a charge neutral system, and the initial wave function is assumed to be strongly confined inside the short range nuclear interaction.

We have extended the MW formula to include the effects of the finite spins, the finite charge, and the finite size of the initial wave packet. First, the numerator of $\sqrt{E}$ is replaced by the penetration factor $P_\lambda(ka)$ depending on the channel radius a to take into account the effects of the finite spin (λ) and the finite charge. This replacement can be justified by the plane wave approximation for the final scattering state. Second, we have introduced the exponential damping factor, $e^{-\beta E}$, in

which β originates from the tunneling tail of the initial wave packet outside of the nuclear interaction approximated by the harmonic oscillator potential. Thus, two parameters are newly introduced in the extended MW formula: the channel radius a and the width of the energy damping β. Both parameters originate from the finite size of the initial wave function.

We have tested the extended MW formula by fitting the background strength evaluated by the theoretical calculation of the direct breakup. Here we have calculated the background strength by the direct breakup on the basis of the formulation of the complex scaling method (CSM) [32], in which the final state interaction after the breakup is fully taken into account. The CSM calculation and the fitting analysis by the extended MW formula are applied to the direct breakup in ^{20}Ne $\rightarrow \alpha + {}^{16}$O [33]. In this application, we have confirmed that the CSM strength functions are nicely reproduced by the extended MW formula. If we switch off the exponential damping part $e^{-\beta E}$ in the fitting, the strength in the higher energy region is overestimated. Thus, both the penetration factor and the exponential damping factor are important to reproduce the background strength over a wide region of the excitation energy.

The sensitivity of β, which is one of new parameters, to the spatial size of the initial wave function is checked by varying the binding energy of the initial state. The longer range wave packet requires large β, which gives rapid damping to the strength function, and there is a positive correlation of β and the root-mean-squared radius of the initial wave function, $\sqrt{\langle R^2 \rangle}$. Although we do not show the results, the channel radius a, which is another new parameter, is also sensitive to the spatial size of the initial wave function. We should be careful that the value of $\sqrt{\langle R^2 \rangle}$ correlating β and a does not correspond to the normal nuclear radius, which is usually derived from the reaction cross section. The nuclear radius is given by the average of $\sqrt{\langle R^2 \rangle}$ for the various channel components contained in the ground state. $\sqrt{\langle R^2 \rangle}$ associated with β and a corresponds to the spatial size of the specific channel component in the ground state.

Finally, the extended MW formula is applied to the direct breakup of ^{12}Be $\rightarrow \alpha + {}^8$He, in which prominent resonances are observed in experiments [8–12]. The strengths for the monopole, dipole, and quadrupole breakups evaluated by the CSM calculation are nicely reproduced by the extended MW formula. Since the CSM calculation reproduces the single peak structure, which is expected in the structureless background strength, it appropriately simulates the nonresonant background strength in the binary breakup. Therefore, the extended MW formula reproducing the CSM result is considered to be a realistic formula to evaluate the nonresonant background strength.

A strict extension of the MW formula must rely on the formal theory of the corrected effective range, which includes the effects of the finite Coulomb potential and the finite angular momentum [47]. However, such an exact extension of the MW formula is quite difficult because of the nonlinear Coulomb effect appearing in the effective range relation [47]. Instead, we have extended the MW formula in an intuitive manner, which finally leads to the simple multiplication of

the quadratic energy denominator and the penetration and damping factors. Since we have demonstrated the availability of the extended MW formula, its application to various binary breakup reactions is strongly desired. Furthermore, it is important to extend the formula to more complicated systems, such as three-body breakup, because experimental data measuring multiparticle decays have been accumulated [7,14–16]. The extension to the three-body breakup is now in progress.

[1] P. Ring and P. Schuck, *Nuclear Many-Body Problem* (Springer-Verlag, Berlin, 2004).

[2] H. Horiuchi *et al.*, Prog. Theor. Phys. Suppl. **192**, 1 (2012), and references therein.

[3] T. Yamada, Y. Funaki, H. Horiuchi, K. Ikeda, and A. Tohsaki, Prog. Theor. Phys. **120**, 1139 (2008).

[4] T. Yamada, Y. Funaki, T. Myo, H. Horiuchi, K. Ikeda, G. Röpke, P. Schuck, and A. Tohsaki, Phys. Rev. C **85**, 034315 (2012).

[5] T. Nakamura *et al.*, Phys. Lett. B **331**, 296 (1994).

[6] T. Nakamura *et al.*, Phys. Rev. Lett. **96**, 252502 (2006).

[7] K. J. Cook, *et al.*, Phys. Rev. Lett. **124**, 212503 (2020).

[8] A. A. Korsheninnikov *et al.*, Phys. Lett. B **343**, 53 (1995).

[9] M. Freer *et al.*, Phys. Rev. Lett. **82**, 1383 (1999); Phys. Rev. C **63**, 034301 (2001).

[10] A. Saito *et al.*, Mod. Phys. Lett. A **25**, 1858 (2010).

[11] R. J. Charity *et al.*, Phys. Rev. C **76**, 064313 (2007).

[12] Z. H. Yang *et al.*, Phys. Rev. Lett. **112**, 162501 (2014).

[13] N. Soić *et al.*, Europhys. Lett. **34**, 7 (1996).

[14] S. Leblond *et al.*, Phys. Rev. Lett. **121**, 262502 (2018).

[15] Y. Kubota *et al.*, Phys. Rev. Lett. **125**, 252501 (2020).

[16] Y. Kondo *et al.*, Phys. Rev. Lett. **116**, 102503 (2016).

[17] M. Kamimura *et al.*, Prog. Theor. Phys. Suppl. **89**, 1 (1986).

[18] S. Watanabe, K. Ogata, and T. Matsumoto, Phys. Rev. C **103**, L031601 (2021).

[19] S. Ogawa and T. Matsumoto, Phys. Rev. C **102**, 021602(R) (2020).

[20] P. Descouvemont, Phys. Rev. C **97**, 064607 (2018).

[21] P. Descouvemont, Phys. Rev. C **101**, 064611 (2020).

[22] M. Ito, N. Itagaki, H. Sakurai, and K. Ikeda, Phys. Rev. Lett. **100**, 182502 (2008).

[23] M. Ito, Phys. Rev. C **85**, 044308 (2012).

[24] M. Ito and N. Itagaki, Phys. Rev. C **78**, 011602(R) (2008).

[25] M. Ito and D. Suzuki, Phys. Rev. C **84**, 014608 (2011).

[26] M. Ito and K. Ikeda, Rep. Prog. Phys. **77**, 096301 (2014).

[27] S. Shimoura, Eur. Phys. J. Plus **133**, 463 (2018).

[28] A. Migdal, Sov. Phys. JETP **1**, 2 (1955).

[29] K. Watson, Phys. Rev. **88**, 1163 (1952).

[30] N. Austern, Nucl. Phys. **7**, 195 (1958).

[31] R. Nakamoto, M. Ito, A. Saito, and S. Shimoura, JAEA Conference report, Proceedings of the 2020 Symposium on Nuclear Data, November 26–27, 2020, RIKEN Wako Campus, Saitama, Japan (to be published).

[32] S. Aoyama, T. Myo, K. Katō, and K. Ikeda, Prog. Theor. Phys. **116**, 1 (2006).

[33] A. T. Kruppa and K. Katō, Prog. Theor. Phys. **84**, 1145 (1990).

[34] T. Myo, A. Ohnishi, and K. Katō, Prog. Theor. Phys. **99**, 801 (1998).

[35] G. R. Satchler, *Direct Nuclear Reactions* (Clarendon, Oxford, 1983), p. 577.

[36] H. Sagawa, N. Takigawa, and N. van Giai, Nucl. Phys. A **543**, 575 (1992).

[37] Y. Chiba, M. Kimura, and Y. Taniguchi, Phys. Rev. C **93**, 034319 (2016).

[38] Y. Chiba, Y. Taniguchi, and M. Kimura, Phys. Rev. C **95**, 044328 (2017).

[39] G. R. Satchler and W. G. Love, Phys. Rep. **55**, 183 (1979).

[40] A. M. Kobos *et al.*, Nucl. Phys. A **384**, 65 (1982); A. M. Kobos, B. A. Brown, R. Lindsay, and G. R. Satchler, *ibid.* **425**, 205 (1984).

[41] M. Ito, Y. Hirabayashi, and Y. Sakuragi, Phys. Rev. C **66**, 034307 (2002), and references therein.

[42] Y. Hirabayashi, Y. Sakuragi, and Y. Abe, Phys. Rev. Lett. **75**, 3779 (1995).

[43] M. Nakao, H. Umehara, S. Sonoda, S. Ebata, and M. Ito, EPJ Web Conf. **163**, 00040 (2017).

[44] F. M. El-Azab and G. R. Satchler, Nucl. Phys. A **438**, 525 (1985).

[45] M. E. Brandan and G. R. Satchler, Nucl. Phys. A **487**, 477 (1988).

[46] H. Friedrich, Phys. Rep. **74**, 209 (1981).

[47] J. Hamilton, I. Øverbö, and B. Tromborg, Nucl. Phys. B **60**, 443 (1973).

[48] F. C. Barker and P. B. Treacy, Nucl. Phys. **38**, 33 (1962).